Supporting Information

Ochaba et al. 10.1073/pnas.1420103111

SI Materials and Methods

Plasmids. pARIS-httpcDNA3.2-N[His-mCherry]Q23-C[HA-TC] (pARIS-mCherry-httQ23), pARIS-httpcDNA3.2-N[His-mCherry] Q100-C[HA-TC] (pARIS-mCherry-httQ100), pcDNA25QP-H4 exon 1, pcDNA97QP-H4 exon 1, pcDNA25Q-586aa and pcDNA137Q-586aa were previously described (1–3). The following plasmids were obtained from Origene: MYC-DDK-GABARAPL1 DNA (RC206762), MYC-DDK-BNIP3L (NIX) DNA (RC203315), MYC-DDK-MAP1LC3B DNA (RC207356). HA-ULK1, MYC-ATG13, MYC-FIP200 and MYC-p62 have been previously described (4, 5). W3037A mutants were made in the full-length HTT gene in pARIS by site directed in vitro mutagenesis. Venus-HTT(2416–3144) and Venus-(1651–3144) were generated fusing Venus in the vector pGW1 in frame with the C-terminal 728 aa of HTT using the pARIS SpeI site, and with the C-terminal 1493aa of HTT using the pARIS SalI site. We inserted a short synthetic oligonucleotide into the BglII-EcoRI site of pGW1 just downstream of the Venus coding sequence: 5′-GATCTGTCGACATTCTAGATATAGAATTCT-GA-3′ 3′-ACAGCTGTAAGATCTATATCTTAAGACTTTAA-5′. These oligonucleotides provided the SalI and the XbaI (that has a complementary 5′ overhang with SpeI) restriction sites in frame with the Venus coding sequence for the insertion of HTT gene fragments and also added a stop codon to terminate the fusion proteins at the 3′ end of the HTT gene. We inserted both the SalI-EcoRI and the SpeI-EcoRI fragments of pARIS-HTT plasmids into pGW1. Using this technique we generated 4 constructs: Venus-HTT(2416–3144) WT, Venus-HTT(2416–3144) W3037A, Venus-HTT(1651–3144) WT, and Venus-HTT(1651–3144) W3037A.

Antibodies. The following antibodies were used: anti-HTT-5492 (Millipore); anti-HA11 Clone 16B12 monoclonal (Covance); anti-MYC 9E10 (Millipore); anti-actin A2066 (Sigma-Aldrich) anti–β-actin (MP Biomedicals), anti–α-Tubulin (Sigma-Aldrich), anti-p62/SQSTM1 (American Research Products), anti-Living Colors (to detect EGFP and Venus) 632592 polyclonal or 632381 monoclonal (Clontech), anti–rabbit-FITC and anti-guinea pig-Cy3 (Jackson Immunologicals). Primary antibodies used for mouse immunohistochemistry were: p62/SQSTM1 (American Research Products) and ubiquitin (Novus). Anti-Ref(2)P was kindly provided by Gabor Juhasz (Eötvös Loránd University, Budapest, Hungary).

Cell Culture and Transfection. HEK293T cells were cultured at 37 °C at 5% CO_2 in DMEM supplemented with 10% (vol/vol) FBS, and were transfected using Lipofectamine 2000 reagent (Invitrogen). 293T cells were harvested for Western analysis 48 h after transfection.

Immunoprecipitation. 293T cells were lysed in buffer containing: 20 mM Tris·HCl, pH 7.5, 10% (vol/vol) glycerol, 137 mM NaCl, 0.5 mM EDTA, 1% Nonidet P-40, supplemented with 20 mM *N*-ethylmaleimide, 1 mM PMSF, phosphatase inhibitors 2 and 3 (Sigma-Aldrich), complete miniprotease inhibitor pellet (Roche), 10 ng/mL aprotenin, 10 ng/mL leupeptin, 5 mM nicotinamide, and 5 mM butyrate. Briefly, transfected cells were harvested, lysed, and sonicated on ice. Next, 500 μg of lysate was incubated with lysis buffer [−10% (vol/vol) glycerol] + phosphatase inhibitors 2 and 3 and added to Dynabeads (Invitrogen) coupled to anti-HA, anti-myc, or anti-Living Colors antibodies and incubated on a rotator overnight at 4 °C. Immunoprecipitates were washed three times and analyzed by Western blot.

Western Blot. Equal amounts of protein were subjected to SDS/PAGE on 4–12% Bis·Tris or 3–8% Tris-acetate minigels (Invitrogen) and transferred onto 0.45-μm nitrocellulose membranes (Bio-Rad). Membranes were incubated with Starting Block–TBS blocking buffer (Thermo Scientific) for 1 h, then with primary antibodies overnight. Blots were washed three times with TBS-0.1% Tween-20 for 8 min and incubated with secondary IgG-HRP antibodies for 45 min, washed three more times, and detected with SuperSignal West Pico Chemiluminescent Substrate or SuperSignal West Dura Extended Duration Substrate (Thermo Scientific) according to the instructions of the supplier. Membranes were exposed to BioMax XAR (Kodak) films and developed. The signal intensities were analyzed and quantitated using ScionImage. Experiments were performed in triplicate or greater with representative images shown.

Statistical Analysis. All statistical analyses were performed using GraphPad Prism 5.04 software. All data are expressed as mean ± SE of measure. $P < 0.05$ was considered to be statistically significant in all cases. Statistical comparisons of results were performed by performing one-way ANOVA analysis followed by Bonferroni's multiple comparison tests.

Primary Cortical Neuron Survival Assay.

Cell culture and transfection. Cortical neurons were dissected from embryonic day 20–21 rat pups and cultured at 0.6×10^6 cells/mL for 4 d in vitro, as described previously (6). For survival analyses, cells were plated at a density of 0.1×10^6 cells per well of a 96-well plate. Euthanasia for these experiments was entirely consistent with the recommendations of the Guidelines on Euthanasia of the American Veterinary Medical Association. Transfection of primary neurons was accomplished using Lipofectamine 2000 (Invitrogen). All transfections involved 0.02–0.7 μg DNA (total) and 0.5 μl Lipofectamine 2000 per well. Cells were incubated with Lipofectamine/DNA complexes for 60 min at 37 °C before rinsing. The remainder of the transfection protocol was per the manufacturer's suggestions, resulting in an overall transfection efficiency of < 1%.

Longitudinal fluorescence microscopy. Experiments involving neuronal survival analysis used an automated microscopy platform described previously (7, 8). Briefly, images were obtained at 24-h intervals with an inverted microscope (Nikon Ti-E) equipped with the PerfectFocus system, a high-numerical aperture 20× objective lens and a 16-bit Andor 888 back-thinned EMCCD digital camera with a cooled charge-coupled device. Illumination was provided by a Lambda XL lamp (Sutter) with a liquid light guide. The MS-2500 XY stage (Applied Scientific) was controlled by rotary encoders in all three planes of movement. All components were encased in a custom-designed, climate-controlled environmental chamber (In Vivo Scientific). The illumination, filter wheels, focusing, stage movements, and image acquisitions were fully automated and coordinated with a mix of proprietary (GreenButtonGo + scheduler + Liconic Incubator) and publicly available (ImageJ, μManager) software.

Image analysis. Relevant data were extracted from the raw, digital images in a sequential process using an original script developed in Accelrys PipelinePilot. Briefly, the median background fluorescence from a portion of all images was calculated and subtracted from individual image. The images were then assembled into montages representing each well at each time point. The montages were sequenced and aligned automatically, and neuron cell bodies segmented based on intensity and morphology. Among the variables recorded for each neuron were the fluorescence intensity and the time of death, marked by the loss of cellular

fluorescence, rounding, or dissolution of the cell body. Statistical analyses and the generation of cumulative hazard plots were accomplished using custom-designed algorithms and the survival package within R, and bar graphs were created using Prism (6–8).

Survival analysis. For longitudinal survival analysis, the survival time of a neuron was defined as the time point at which a cell was last seen alive. Survival functions were fitted to Kaplan–Meier curves and used to derive cumulative hazard (or risk-of-death) curves that describe the instantaneous risk-of-death for individual neurons in the cohort being tracked. We used Cox proportional hazards regression analysis (Cox analysis) to generate hazard ratios that quantified the relative risk-of-death between cohorts of neurons expressing different constructs. Hazard ratios and their respective *P* values were generated using the *coxph* function in the survival package for R statistical software. The date of the experiment was included as a stratification variable and expression of each construct at the first time point was included as a covariate. All Cox models were analyzed for violations of proportional hazards using the *cox.zph* function in R.

***Nestin-cre* Conditional *Htt* Knockout Mouse.** For conditional knockout of *Htt* expression in neuronal progenitors, we used a *nestin-cre* transgenic line (9). $Htt^{flox/-}$;*nestin-cre-tg* mice were obtained from crosses between $Htt^{+/-}$; *nestin-cre-tg* males and $Htt^{flox/flox}$ females. Cre-mediated recombination begins ∼ embryonic day 9.5, and HTT expression is eliminated in neuronal progenitors and their differentiated progeny (neurons and glia). Brains from $Htt^{flox/-}$;*nestin-cre-tg* and $Htt^{flox/+}$;*nestin-cre-tg* controls or CAG140 heterozygous HD knockin mice (10) were rapidly frozen in isopentane chilled on dry ice, and then 14-μm fresh frozen sections through the striatum were obtained using a cryostat (Bright Instrument). Sections were washed briefly in PBS, fixed for 10 min in 4% (vol/vol) paraformaldehyde for 10 min, followed by a rinse in PBS and then a second fixation step in 100% methanol for 15 min on ice. Sections were then washed again in PBS before blocking with 5% (vol/vol) donkey serum, 0.1% Triton X-100 in PBS for 1 h at room temperature, and then incubated overnight at 4 °C with primary antibody diluted in 5% (vol/vol) donkey serum, 0.1% Triton X-100 in PBS. Primary antibodies used were: p62/SQSTM1 (1:100 guinea pig polyclonal from American Research Products) and ubiquitin (1:100 rabbit polyclonal from Novus). Following the primary antibody incubation, sections were washed in PBS three times and incubated with secondary antibodies (anti–rabbit-FITC and anti-guinea pig-Cy3; Jackson Immunologicals), together with the fluorescent DNA stain To-Pro-3 iodide (1:10,000; Invitrogen) for 1 h at room temperature. Lipofuscin autofluorescence was suppressed by washing with PBS, and then incubating sections sequentially in 75% (vol/vol) ethanol for 5 min, lipofuscin eliminator reagent (Millipore) for 5 min, and 5 min in 75% (vol/vol) ethanol. Sections were then mounted with Vectashield (Vector Laboratory, and examined using either an Olympus BX51 microscope equipped with a MagnaFire CCD camera or a Nikon C1-confocal microscope). p62/SQSTM1 was detected by Western analysis in the striatal pellet fraction and quantitated as previously described (11).

Lipofuscin analysis was performed using 14-μm fresh-frozen brain sections. Sections were fixed for 15 min on ice in 100% methanol, washed in PBS, and then incubated with To-Pro-3 iodide (1:10,000 dilution in PBS) for 1 h at room temperature. Sections were then washed in PBS and mounted using Vectashield. Lipofuscin autofluorescence was imaged in the green and red channels (lipofuscin has a broad emission spectrum from 500 nm to 650 nm).

***Drosophila* HTT LOF Experiments.**

Drosophila *stocks.* Stocks were maintained on a standard cornmeal/sugar/agar medium at 25 °C and 50% humidity on a 12-h light/12-h dark cycle. To obtain a large amount of synchronized larvae, first the well-fed adults were transferred into new vials and allowed to lay their eggs for 1 h. After this prelaying period, the flies were transferred again into new vials for egg laying for 3 h. This second collection contained fertilized eggs, which gave larvae with relatively synchronized stages with regard to development.

Starvation treatments. Early third-instar larvae synchronized at 88 h after egg laying were floated in 20% (wt/vol) sucrose for 3 h at room temperature (12).

LysoTracker Red staining. Treated (starved) and nontreated larvae were dissected in 100 μL PBS and stained in 100 μM LTR (Invitrogen, L7528) diluted in PBS for 3 min. After washing the tissues were mounted in 50% (vol/vol) glycerol/PBS completed with 1 μg/μL DAPI (Sigma, D9542).

p62 immunostaining. A polyclonal affinity-purified p62/Ref(2)P antibody (raised in rabbit) was used in this experiment (kindly provided by Gabor Juhasz, Eötvös Loránd University, Budapest, Hungary). Fat bodies from synchronous 88 h after egg laying starved third-instar larvae were dissected and fixed with 3.6% (vol/vol) formaldehyde in PBS for 60 min at room temperature. Samples were washed 2× 5 min in PBS then were incubated for 20 min in PBS + 0.1% Triton X-100. Following 3× 5-min wash with PBS, nonspecific binding sites were blocked by incubation with 3% (wt/vol) milk powder dissolved in PBS for 1 h. Incubations with primary and secondary antibodies were performed overnight at 4 °C and for 1 h at room temperature, respectively, in the blocking buffer diluted 1:1 with PBS. Primary antibodies were used at a dilution of 1:2,000. Anti-rabbit-Alexa488 (Invitrogen) secondary antibody was used at a dilution of 1:1,400.

Microscopy. Images were obtained on a fluorescent microscope (Carl Zeiss, Axioimager 2.1) equipped with a grid confocal unit (Carl Zeiss, Apotome) using Plan-NeoFluar 40× 0.75 NA air objective (Carl Zeiss), Axiocam Mrm camera (Carl Zeiss) and Axiovision software (Carl Zeiss).

Climbing assay. Just after onset of pupariation, the distance between the surface of food and the middle point of five puparium located furthest from the food were measured. The average was considered as the representative highest distance for that given culture. Ten vials of control and HTT LOF lines were measured and the average values were presented in mm on the diagram. Both synchronous and nonsynchronous *Drosophila* cultures were kept under similar conditions.

1. Pardo R, et al. (2010) pARIS-htt: An optimised expression platform to study huntingtin reveals functional domains required for vesicular trafficking. *Mol Brain* 3:17.
2. Thompson LM, et al. (2009) IKK phosphorylates Huntingtin and targets it for degradation by the proteasome and lysosome. *J Cell Biol* 187(7):1083–1099.
3. O'Rourke JG, et al. (2013) SUMO-2 and PIAS1 modulate insoluble mutant huntingtin protein accumulation. *Cell Reports* 4(2):362–375.
4. Jung CH, et al. (2009) ULK-Atg13-FIP200 complexes mediate mTOR signaling to the autophagy machinery. *Mol Biol Cell* 20(7):1992–2003.
5. Wooten MW, et al. (2008) Essential role of sequestosome 1/p62 in regulating accumulation of Lys63-ubiquitinated proteins. *J Biol Chem* 283(11): 6783–6789.
6. Saudou F, Finkbeiner S, Devys D, Greenberg ME (1998) Huntingtin acts in the nucleus to induce apoptosis but death does not correlate with the formation of intranuclear inclusions. *Cell* 95(1):55–66.
7. Arrasate M, Mitra S, Schweitzer ES, Segal MR, Finkbeiner S (2004) Inclusion body formation reduces levels of mutant huntingtin and the risk of neuronal death. *Nature* 431(7010):805–810.
8. Barmada SJ, et al. (2010) Cytoplasmic mislocalization of TDP-43 is toxic to neurons and enhanced by a mutation associated with familial amyotrophic lateral sclerosis. *J Neurosci* 30(2):639–649.
9. Tronche F, et al. (1999) Disruption of the glucocorticoid receptor gene in the nervous system results in reduced anxiety. *Nat Genet* 23(1):99–103.
10. Menalled LB, Sison JD, Dragatsis I, Zeitlin S, Chesselet MF (2003) Time course of early motor and neuropathological anomalies in a knock-in mouse model of Huntington's disease with 140 CAG repeats. *J Comp Neurol* 465(1):11–26.
11. Zheng S, et al. (2010) Deletion of the huntingtin polyglutamine stretch enhances neuronal autophagy and longevity in mice. *PLoS Genet* 6(2):e1000838.
12. Neufeld TP (2008) Genetic manipulation and monitoring of autophagy in *Drosophila*. *Methods Enzymol* 451:653–667.

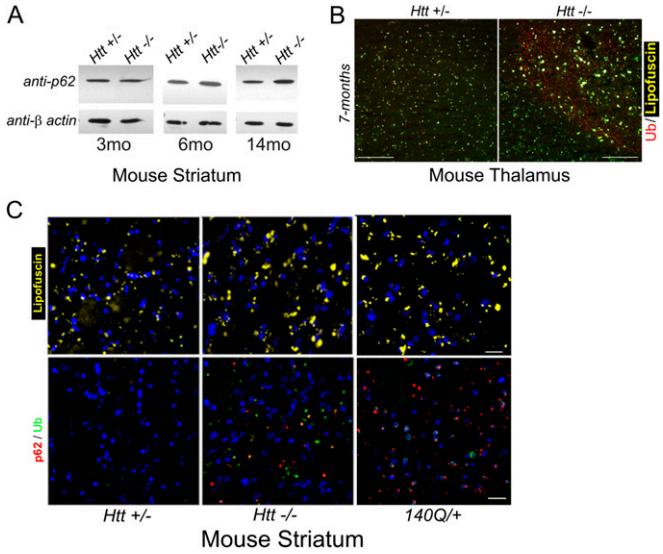

Fig. S1. p62, lipofuscin and ubiquitin accumulate in Htt knockout mouse brain. (*A*) *Htt*$^{flox/-}$;*nestin-cre-tg* CNS conditional *Htt* knockout mice (Htt$^{-/-}$) significantly accumulate p62/SQSTM1 in the striatal insoluble fraction with aging, as shown by Western blot. (*B*) Lipofuscin and ubiquitin accumulate in *Htt*$^{flox/-}$;*nestin-cre-tg* CNS conditional *Htt* knockout mouse thalamus at 7 mo. Confocal images of the thalamus of *Htt*$^{flox/+}$;*nestin-cre* (Htt$^{+/-}$ controls) and *Htt*$^{flox/-}$;*nestin-cre* (Htt$^{-/-}$) conditional knockout mice. Increased lipofuscin autofluorescence in the green and red channels (yellow) and ubiquitin puncta (red) are evident in the mutant thalamus. (Scale bar, 159.13 μm.) (*C*) Two-year old *Htt*$^{flox/-}$;*nestin-cre-tg* CNS conditional *Htt* knockout mice and heterozygous CAG140 HD knockin mice accumulate lipofuscin and neuropil protein aggregates that can contain ubiquitin or p62/SQSTM1 in the striatum. (Scale bar, 25 μm.)

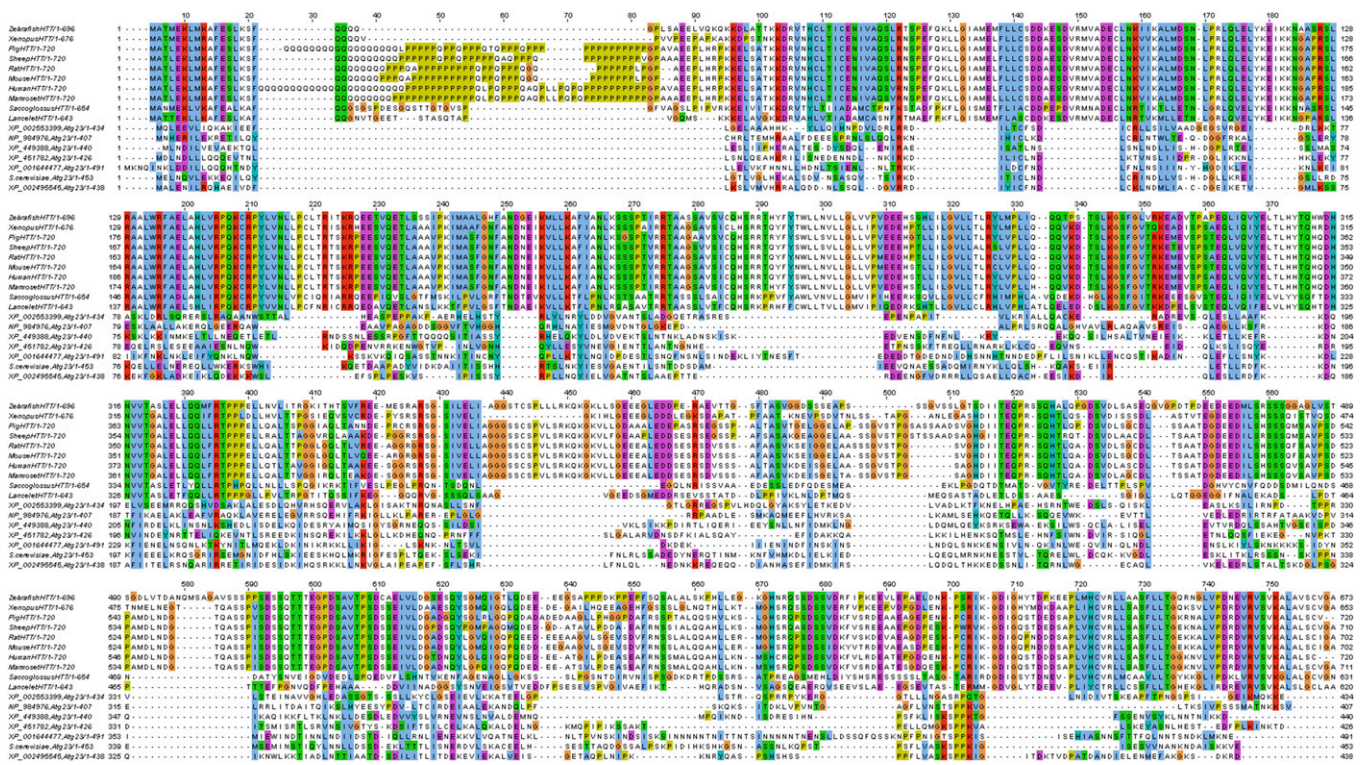

Fig. S2. Alignment of the N-terminal domain of HTTs with yeast Atg23s. The alignment was done using EMBL-EBI MUltiple Sequence Comparison by Log-Expectation (MUSCLE, www.ebi.ac.uk/Tools/msa/muscle) (1, 2) and Jalview Java Alignment Editor (3, 4).

1. Edgar RC (2004) MUSCLE: A multiple sequence alignment method with reduced time and space complexity. *BMC Bioinformatics* 5:113.
2. Edgar RC (2004) MUSCLE: Multiple sequence alignment with high accuracy and high throughput. *Nucleic Acids Res* 32(5):1792–1797.
3. Clamp M, Cuff J, Searle SM, Barton GJ (2004) The Jalview Java alignment editor. *Bioinformatics* 20(3):426–427.
4. Waterhouse AM, Procter JB, Martin DM, Clamp M, Barton GJ (2009) Jalview Version 2—A multiple sequence alignment editor and analysis workbench. *Bioinformatics* 25(9):1189–1191.

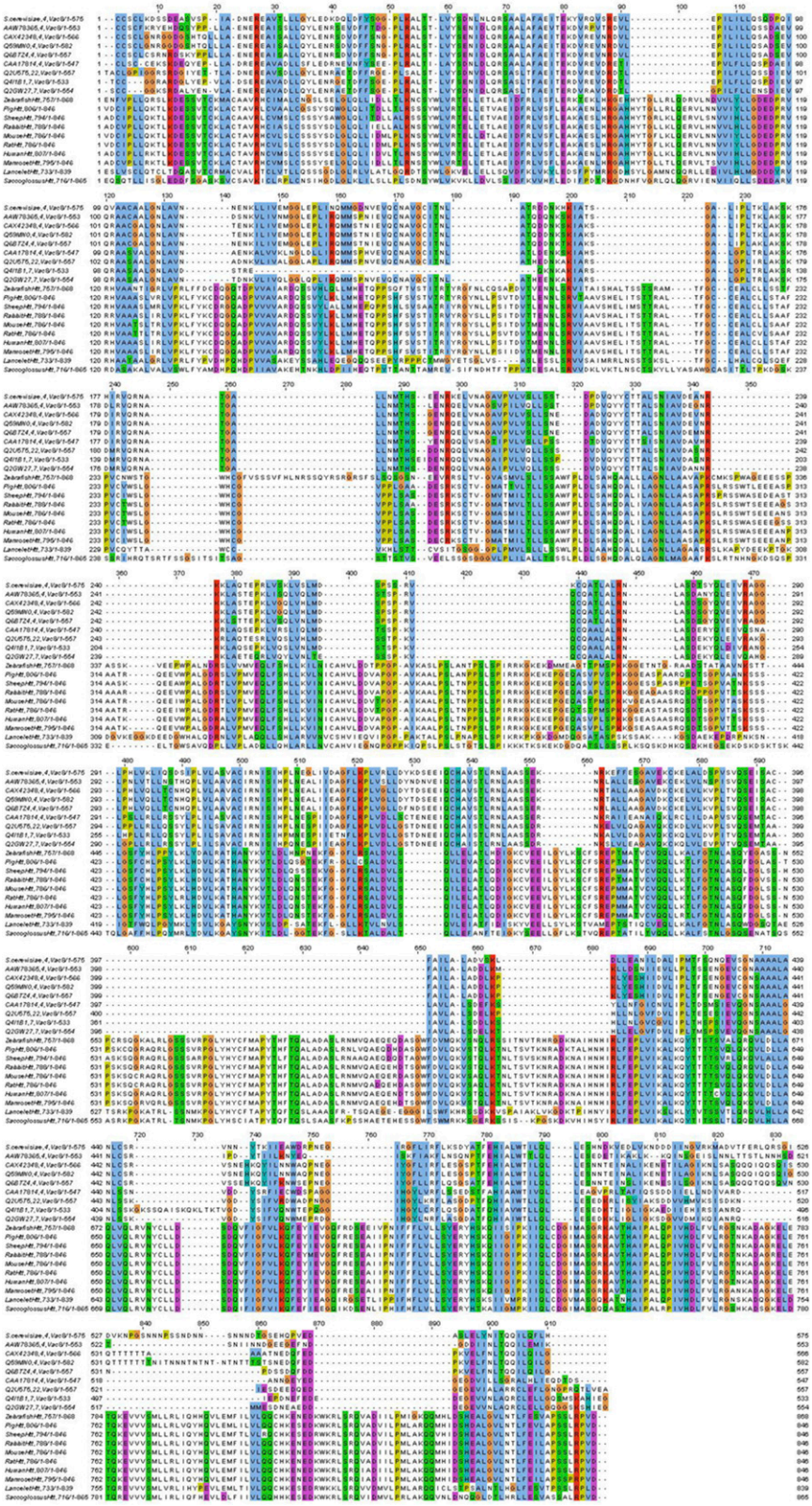

Fig. S3. Alignment of the central domain of HTTs with yeast Vac8s. The alignment was done using EMBL-EBI MUltiple Sequence Comparison by Log-Expectation (MUSCLE, www.ebi.ac.uk/Tools/msa/muscle) (1, 2) and Jalview Java Alignment Editor (3, 4).

1. Edgar RC (2004) MUSCLE: A multiple sequence alignment method with reduced time and space complexity. *BMC Bioinformatics* 5:113.
2. Edgar RC (2004) MUSCLE: Multiple sequence alignment with high accuracy and high throughput. *Nucleic Acids Res* 32(5):1792–1797.
3. Clamp M, Cuff J, Searle SM, Barton GJ (2004) The Jalview Java alignment editor. *Bioinformatics* 20(3):426–427.
4. Waterhouse AM, Procter JB, Martin DM, Clamp M, Barton GJ (2009) Jalview Version 2—A multiple sequence alignment editor and analysis workbench. *Bioinformatics* 25(9):1189–1191.

Fig. S4. Alignment of the C-terminal domain of HTTs with yeast Atg11s. The alignment was done using EMBL-EBI MUltiple Sequence Comparison by Log-Expectation (MUSCLE, www.ebi.ac.uk/Tools/msa/muscle) (1, 2) and Jalview Java Alignment Editor (3, 4).

1. Edgar RC (2004) MUSCLE: A multiple sequence alignment method with reduced time and space complexity. *BMC Bioinformatics* 5:113.
2. Edgar RC (2004) MUSCLE: Multiple sequence alignment with high accuracy and high throughput. *Nucleic Acids Res* 32(5):1792–1797.
3. Clamp M, Cuff J, Searle SM, Barton GJ (2004) The Jalview Java alignment editor. *Bioinformatics* 20(3):426–427.
4. Waterhouse AM, Procter JB, Martin DM, Clamp M, Barton GJ (2009) Jalview Version 2—A multiple sequence alignment editor and analysis workbench. *Bioinformatics* 25(9):1189–1191.

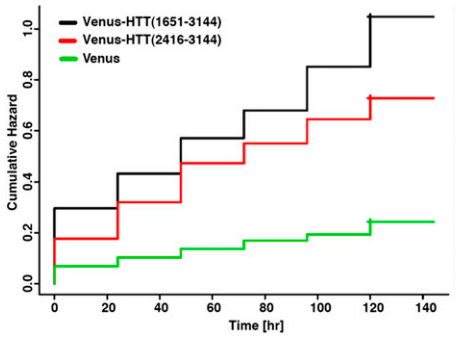

Group	HR	95% CI	*p* value
Venus-HTT(1651-3144) (*n* = 499) vs. Venus (*n* = 602)	13.6	(8.84-20.9)	$< 2x10^{-16}$
Venus-HTT(2416-3144) (*n* = 383) vs. Venus (*n* = 602)	8.56	(5.78-12.7)	$< 2x10^{-16}$

Fig. S5. The C-terminal domain of HTT is toxic in primary cortical neurons. Venus-HTT(1651–3144) and Venus-HTT(2416–3144) expression reduces survival of rat primary cortical neurons. Kaplan–Meier plots are shown for survival analysis performed on primary rat cortical neurons. The table shows the results of a Cox proportional hazards analysis performed to compare survival across groups expressing different Venus constructs. Initial expression level of each construct was included as a covariate to account for differences in expression level between Venus constructs. CI, Confidence interval; HR, hazard ratio; *n*, number of neurons.

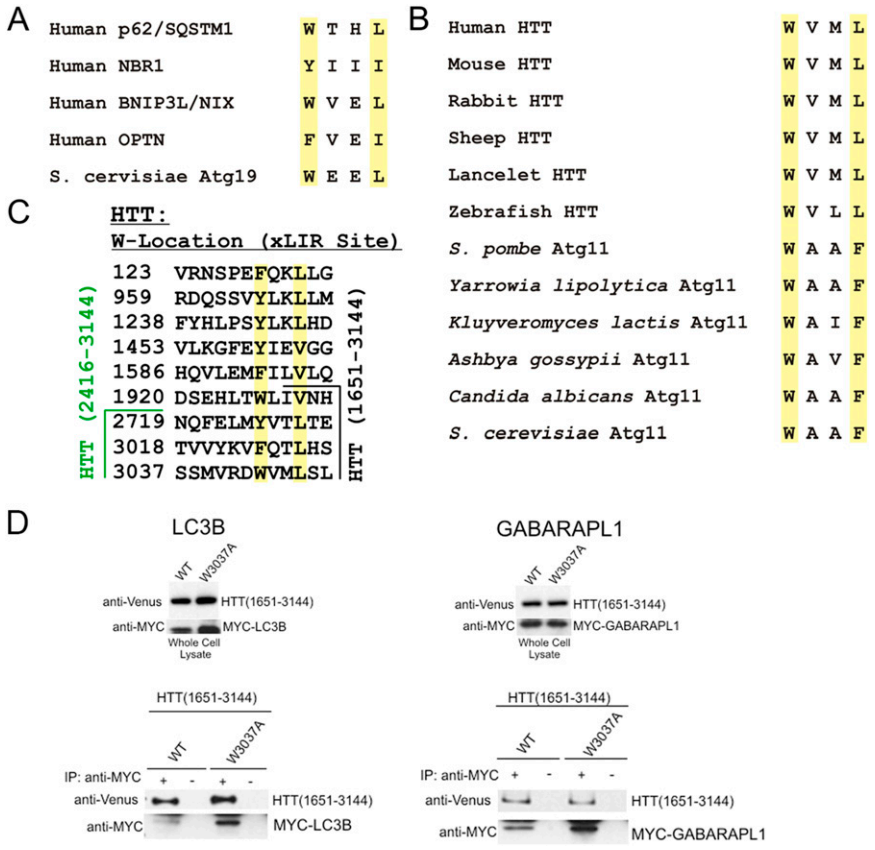

Fig. S6. HTT contains a conserved WXXL domain at W3037 (*A*) Published WXXL domains shown to interact with the Atg8 family of proteins. (*B*) WXXL domain conserved between HTT and Atg11 families, aligned with W3037 of human HTT. (*C*) xLIRs defined in human HTT using iLIR web resource(1). (*D*) Venus-HTT(1651-3144) fusion protein coimmunoprecipitates with mammalian Atg8s. HEK293T cells were cotransfected with Venus-HTT(1651–3144) and MYC-LC3B or MYC-GABARAPL1. Cell lysates were subjected to immunoprecipitation (using anti-MYC). The resulting precipitates were examined by immunoblot analysis with the indicated antibodies. W3037A mutation does not reduce binding of the longer HTT C-terminal fragment, Venus-HTT(1651–3144) to MYC-GABARAPL1 or MYC-LC3B.

1. Kalvari I, et al. (2014) iLIR: A web resource for prediction of Atg8-family interacting proteins. *Autophagy* 10(5):913–925.

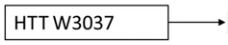

MOTIF	START	END	LIR sequence	PSSM score
xLIR	119	124	PEFQKL	11 (1.5e-01)
xLIR	959	964	SVYLKL	8 (3.9e-01)
xLIR	1234	1239	PSYLKL	11 (1.5e-01)
xLIR	1479	1484	FEYIEV	13 (7.9e-02)
xLIR	1586	1591	EMFILV	10 (2.0e-01)
xLIR	1916	1921	LTWLIV	16 (3.0e-02)
xLIR	2719	2724	LMYVTL	12 (1.1e-01)
xLIR	3018	3023	KVFQTL	7 (5.3e-01)
xLIR	3033	3038	RDWVML	25 (1.7e-03)

Fig. S7. xLIRs in human Huntingtin.

MOTIF	START	END	LIR sequence	PSSM score	MOTIF	START	END	LIR sequence	PSSM score
WxxL	9	14	KAFESL	8 (3.9e-01)	WxxL	1636	1641	TLFEIL	7 (5.3e-01)
WxxL	169	174	ELYKEI	7 (5.3e-01)	WxxL	1790	1795	GMFRRI	6 (7.4e-01)
WxxL	188	193	WRFAEL	2 (2.6e+00)	WxxL	1810	1815	GSFYTL	8 (3.9e-01)
WxxL	286	291	YFYSWL	-1 (6.9e+00)	WxxL	1834	1839	LLWCQI	7 (5.3e-01)
WxxL	588	593	NQYLGL	6 (7.4e-01)	WxxL	1849	1854	RWWAEV	10 (2.0e-01)
WxxL	729	734	SFFSKL	4 (1.4e+00)	WxxL	1999	2004	TPFRVL	4 (1.4e+00)
WxxL	840	845	SSYSEL	11 (1.5e-01)	WxxL	2054	2059	RLYSLL	6 (7.4e-01)
WxxL	859	864	SSYWLV	7 (5.3e-01)	WxxL	2098	2103	DWYVHL	10 (2.0e-01)
WxxL	875	880	IDFRLV	8 (3.9e-01)	WxxL	2200	2205	AYWSKL	11 (1.5e-01)
WxxL	895	900	HHYTGL	4 (1.4e+00)	WxxL	2213	2218	ALYQSL	7 (5.3e-01)
WxxL	985	990	RGYNLL	9 (2.8e-01)	WxxL	2226	2231	AQYLVV	9 (2.8e-01)
WxxL	1076	1081	SAWFPL	12 (1.1e-01)	WxxL	2260	2265	LSWHLI	13 (7.9e-02)
WxxL	1124	1129	EVWPAL	10 (2.0e-01)	WxxL	2290	2295	GLWSVV	11 (1.5e-01)
WxxL	1140	1145	QLFSHL	3 (1.9e+00)	WxxL	2406	2411	NSYTRV	8 (3.9e-01)
WxxL	1228	1233	GSFYHL	7 (5.3e-01)	WxxL	2430	2435	TAFPEI	3 (1.9e+00)
WxxL	1326	1331	SQFDGL	8 (3.9e-01)	WxxL	2466	2471	ETWATL	16 (3.0e-02)
WxxL	1388	1393	SGWFDV	14 (5.7e-02)	WxxL	2575	2580	QAWDPV	13 (7.9e-02)
WxxL	1423	1428	RLFEPL	8 (3.9e-01)	WxxL	2835	2840	TAFYLI	3 (1.9e+00)
WxxL	1460	1465	VNYCLL	4 (1.4e+00)	WxxL	2960	2965	VLFDRI	4 (1.4e+00)
WxxL	1477	1482	KQFEYI	8 (3.9e-01)	WxxL	3089	3094	NLFCLV	0 (5.0e+00)
WxxL	1496	1501	NIFFFL	3 (1.9e+00)	WxxL	3110	3115	RAFQSV	7 (5.3e-01)
WxxL	1579	1584	IQYHQV	2 (2.6e+00)	WxxL	3124	3129	SPYHRL	5 (1.0e+00)
WxxL	1601	1606	DKWKRL	15 (4.2e-02)					

Fig. S8. WXXLs in human Huntingtin.

MOTIF	START	END	LIR Sequence	PSSM Score
xLIR	338	343	ESFEVL	13 (7.9e-02)
xLIR	800	805	GDYDDV	15 (4.2e-02)
xLIR	950	955	PVFQKL	6 (7.4e-01)
xLIR	957	962	DEYELI	16 (3.0e-02)
WxxL	39	44	DFFVSL	9 (2.8e-01)
WxxL	75	80	SMFKEL	10 (2.0e-01)
WxxL	97	102	RLFSLV	4 (1.4e+00)
WxxL	168	173	LNYHSV	5 (1.0e+00)
WxxL	192	197	HYFKSL	2 (2.6e+00)
WxxL	207	212	RIFDGL	6 (7.4e-01)
WxxL	216	221	SQYLKL	10 (2.0e-01)
WxxL	269	274	QKFINI	5 (1.0e+00)
WxxL	306	311	ASFRDI	7 (5.3e-01)
WxxL	392	397	ALYSQI	4 (1.4e+00)
WxxL	448	453	VEFAQV	4 (1.4e+00)
WxxL	466	471	EKYRRL	6 (7.4e-01)
WxxL	472	477	SWFQQI	5 (1.0e+00)
WxxL	504	509	KNFGSI	5 (1.0e+00)
WxxL	521	526	SDFKRL	12 (1.1e-01)
WxxL	590	595	KRFHII	5 (1.0e+00)
WxxL	643	648	FQYSDI	8 (3.9e-01)
WxxL	860	865	EKFETI	11 (1.5e-01)
WxxL	887	892	RIFDII	9 (2.8e-01)
WxxL	997	1002	RRFKDI	6 (7.4e-01)
WxxL	1063	1068	SSFSSV	8 (3.9e-01)
WxxL	1163	1168	SVWFQV	9 (2.8e-01)
WxxL	1173	1178	VSYQGV	6 (7.4e-01)

Fig. S9. xLIRs and WXXL domains in *Saccharomyces cerevisiae* Atg11. PSSM, position-specific scoring matrix.

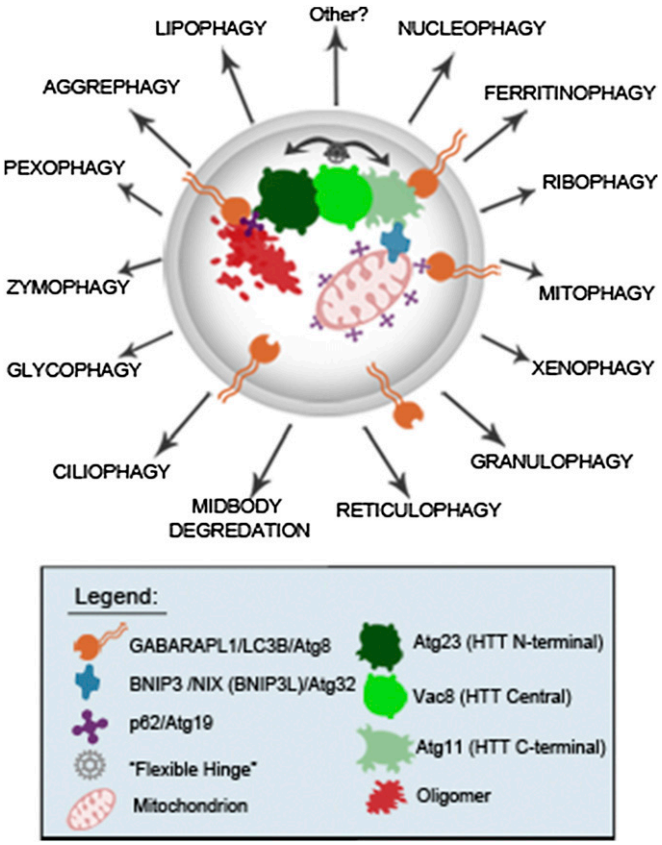

Fig. S10. Theoretical model of HTT as a scaffold protein required for selective autophagy. Functioning as a mammalian Atg11, HTT interacts with receptor proteins (e.g., p62, BNIP3, BNIP3L/NIX) and with ATG8s (e.g., LC3B, GABARAPL1) to enable various forms of selective autophagy.